ORIGINAL ARTICLE

Association of dry skin with intercellular lipid composition of stratum corneum after erlotinib administration

Tomonobu Uchino[1,2] · Hiyori Fujino[1] · Daichi Kamiya[1] · Tomonori Suzuki[1] · Yasunori Miyazaki[1,2] · Kazuhiro Asada[3] · Toshihiro Shirai[3] · Hiroaki Yagi[4] · Yuko Sano[4] · Mutsumi Moriki[4] · Hajime Mizuno[5] · Kenichiro Todoroki[5] · Midori Kimura[6] · Yoshiyuki Kagawa[1,2]

Abstract

Purpose Erlotinib, an inhibitor of the epidermal growth factor receptor tyrosine kinase, causes skin disorders such as dry skin, which impairs the skin barrier function. Stratum corneum (SC) lipids play an important role in skin barrier function; therefore, this study aimed to investigate the relationship between erlotinib-related dry skin and changes in the intercellular lipid composition and structure of the SC.
Methods Overall, 21 patients with non-small lung cancer were enrolled in this study. All patients received 150 mg/day erlotinib orally. A SC sample of each patient was collected from the inner forearm using the tape stripping method on days 0, 7, 14, 28, and 56 after erlotinib administration. The intercellular lipid components of ceramide (CER), free fatty acid (FFA), and cholesterol sulfate (CS) in samples extracted from the tape were analyzed using liquid chromatography/time-of-flight/mass spectrometry. SC samples from six healthy subjects were collected as controls on days 0, 28 and 56 and analyzed similarly.
Results Although total CER and FFA levels were not changed after erlotinib administration, the levels of CER subclasses [AP] and [AH] and hydroxy FFA, which are structural components of CER subclass [A], decreased. In contrast, the CS levels increased after erlotinib administration. Moreover, higher CS levels in the SC correlated with the clinical condition of dry skin. No changes were observed in the SC lipid composition in healthy subjects.
Conclusion Erlotinib-related dry skin was associated with a higher CS level in the SC.

Keywords Erlotinib · Dry skin · Stratum corneum · Cholesterol sulfate · Ceramide · Hydroxy free fatty acid

✉ Tomonobu Uchino
uchinot@u-shizhuoka-ken.ac.jp

1 Laboratory of Clinical Pharmaceutics, School of Pharmaceutical Sciences, University of Shizuoka, 52-1 Yada, Suruga-ku, Shizuoka, Japan

2 Laboratory of Clinical Pharmacokinetics, the Medical Frontier Center, Shizuoka General Hospital, 4-27-1 Kita Ando Aoi-ku, Shizuoka, Japan

3 Department of Respiratory Medicine, Shizuoka General Hospital, 4-27-1 Kita Ando Aoi-ku, Shizuoka, Japan

4 Department of Dermatology, Shizuoka General Hospital, 4-27-1 Kita Ando Aoi-ku, Shizuoka, Japan

5 Laboratory of Analytical and Bio-Analytical Chemistry, School of Pharmaceutical Sciences, University of Shizuoka, 52-1 Yada, Suruga-ku, Shizuoka, Japan

6 Department of Pharmacy, Shizuoka General Hospital, 4-27-1 Kita Ando Aoi-ku, Shizuoka, Japan

Introduction

The epidermal growth factor receptor (EGFR) belongs to a family of tyrosine kinase receptors that regulate cell differentiation, survival, and proliferation. Abnormal EGFR function leads to tumorigenesis [1]. Abnormal EGFR signaling can be inhibited by the monoclonal antibodies cetuximab, panitumumab, and lapatinib, and small-molecule tyrosine kinase inhibitors (TKIs), including erlotinib and gefitinib [2].

Although EGFR-TKIs are widely used to treat several kinds of cancer, skin disorders such as rash, pruritus, dry skin, and acne are among the most common adverse conditions observed in patients treated with these drugs [3]. These conditions can worsen patients' quality of life and lead to dose reduction or discontinuation of treatment. Moreover, the onset times vary among symptoms associated with various skin disorders. An acne-like skin rash and pruritus develop 1–2 weeks after EGFR-TKI treatment initiation,

while dry skin condition develops after 2–3 weeks. In contrast, skin fissures/cracks and/or paronychia occur after 1–2 months [4, 5].

In normal healthy skin, the upper layer of the epidermis, the stratum corneum (SC), protects against external aggressions, such as pollutants, chemicals, or micro-organisms [6]. The SC is composed of corneocytes, which are terminally differentiated keratinocytes devoid of nuclei, surrounded by a lipid matrix, that is essential for the maintenance of skin barrier permeability [7]. The lipids are organized in regularly stacked lipid layers [8]. Within these layers, they adopt dense and highly ordered lateral packing referred to as orthorhombic organization, although a less dense lipid subpopulation is also present in a hexagonal or liquid organization [9]. The lipid matrix is composed of cholesterol, ceramide (CER), and free fatty acids (FFAs) in an equimolar ratio [10, 11]. Additionally, cholesterol sulfate (CS), the sulfate adduct of cholesterol, is also present in intercellular SC lipids [12].

Dry skin, a common skin disease characterized by rough, scaly, or flaky skin, is accompanied by a loss of skin elasticity and relatively frequent pruritus, compared to healthy normal skin [13]. Changes in lipid organization and the decrease in the levels of three CER subclasses are observed in patients with dry skin, depending on the grade of severity [14]. Some diseases such as atopic dermatitis, lamellar ichthyosis, and Gaucher disease also involve changes in the skin barrier [15]. The pathological states of these diseases are manifested by dry skin, changes in lipid composition and packing, and a breakdown of the skin barrier function. Smeden et al. reported that the increase in short-chain CER and FFA levels and the decrease in ultra-long-chain CER levels were correlated with altered lipid organization and decreased barrier function in the SC in patients with atopic dermatitis and Netherton syndrome [16].

Many studies have reported a relationship between the EGFR inhibition and the development of cutaneous side effects [17, 18]. The inhibition of EGFR-mediated signaling pathways induces multiple effects in basal keratinocytes, including growth arrest, decreased migration, increased cell attachment, abnormal differentiation, apoptosis, and stimulation of inflammatory processes, all of which cause distinctive cutaneous manifestations [18, 19]. As EGFR-TKIs inhibits several signaling pathways, including those controlling skin integrity, skin treated with EGFR-TKIs may differ from normal dry skin in terms of lipid composition. Therefore, this study aimed to investigate changes in the composition of intercellular SC lipids after the administration of EGFR-TKIs. Erlotinib, which is used to treat non-small-cell lung cancer, was selected as a representative drug model of EGFR-TKIs.

Materials and methods

Patients and treatments

Twenty-one patients with non-small-cell lung cancer who visited the Department of Respiratory Medicine at Shizuoka General Hospital and were administrated erlotinib from February 2016 to July 2018 were enrolled in this study. Within seven days after the start of erlotinib treatment, three patients were observed for the hepatic toxicity, interstitial lung disease and deterioration of the general condition, respectively. Eighteen patients were finally examined since these three patients were excluded from this study. The Institutional Review Boards of Shizuoka General Hospital (approval number: SGH 14-09-35) and the University of Shizuoka (approval number: 29-47) approved this study protocols. All subjects signed informed consent. None of the subjects had any known history of skin diseases before erlotinib administration. All patients received erlotinib orally (150 mg/day). Bevacizumab, a vascular endothelial growth factor inhibitor, was co-administered in five patients. No renal and hepatic toxicities were observed in any patient during the treatment. The characteristics of the patients are shown in Online Resource Table S1 (Online Resource 1).

The conditions of dry skin and skin rash after the initiation of erlotinib administration were diagnosed by dermatologists according to the Common Terminology Criteria for Adverse Events (CT-CAE) version 4.0 on days 1, 7, 14, 28, and 56. After the diagnosis, five SC samples were collected from the same position of the inner forearm using a commercialized tape patch, D-squame (PROMOTOOL, Tokyo, Japan), on the same day.

For the control group, five SC samples were collected using the same method on days 0, 28, and 56 from six healthy volunteers in their 50 and 60 s. The Institutional Review Board of the University of Shizuoka (approval number: 28-41) approved the protocol for this study.

Stratum corneum samples collection

SC samples were obtained from the inner forearm using the tape stripping method on days 0, 7, 14, 28, and 56 after the initiation of erlotinib. In this study, each tape was pressed against the skin with standardized pressure for 10 s using a standardized pressurizer (D500-D-squame® pressure instrument, PROMOTOOL, Tokyo, Japan) to minimize the pressure associated with sampling [20]. After extracting the intercellular SC lipid components (CER, FFA, and CS) with an organic solvent, the samples were analyzed using ultraperformance liquid chromatography combined with time-of-flight mass spectrometry (UPLC-TOFMS). The data were evaluated comprehensively and

compared with the clinical data. SC samples were stored at − 80 °C until further analysis.

CER and FFA classification

This study applied the most recently introduced CER classification system proposed by Motta et al. [21], that was extended by Masukawa et al. [22]. Figure S1 shows the basic structure of CER and their respective fatty acid and sphingosine chain subclasses. CERs consist of either a dihydrosphingosine (dS), sphingosine (S), phyto-sphingosine (P), or 6-hydroxy sphingosine (H) base. This base is chemically linked to either a non-hydroxy fatty acid (N), α-hydroxy fatty acid (A), or an esterified ω-hydroxy fatty acid (EO). Therefore, 12 CERs subclasses exist with all possible combinations between FAs and sphingosine chains, denoted as: [NS], [NdS], [NP], [NH], [AS], [AdS], [AP], [AH], [EOS], [EOP], [EOH], and [EOdS]. Both chains show a wide distribution in their carbon chain length. Figure 1 shows an overview of

the molecular structures of all known CER subclasses based on the previous reports [16, 22].

Considering the fragmentation studies on CER species in this report, a more detailed nomenclature was used, and the corresponding information was also presented in parentheses to indicate the number of carbon atoms for the specific ester, fatty acid, or carbon chain. For example, CER [E(18:2) O(30)S(18)] corresponds to a CER species containing C18 sphingosine carbon backbone linked via an amide bond to a aω-hydroxy triacontanoic acid, which is ester-linked to a linoleic moiety.

Chemicals

Standards of CERs [N (16) S (18)], [N (18) S (18)], [N (22) S (18)], [N (24) S (18)], [A (16) S (18)], [A (22) S (18)], [A (24) S (18)], [N (16) dS (18)], and [N (24) dS (18)] were purchased from Avanti Polar Lipids, Inc. (Alabama, USA).
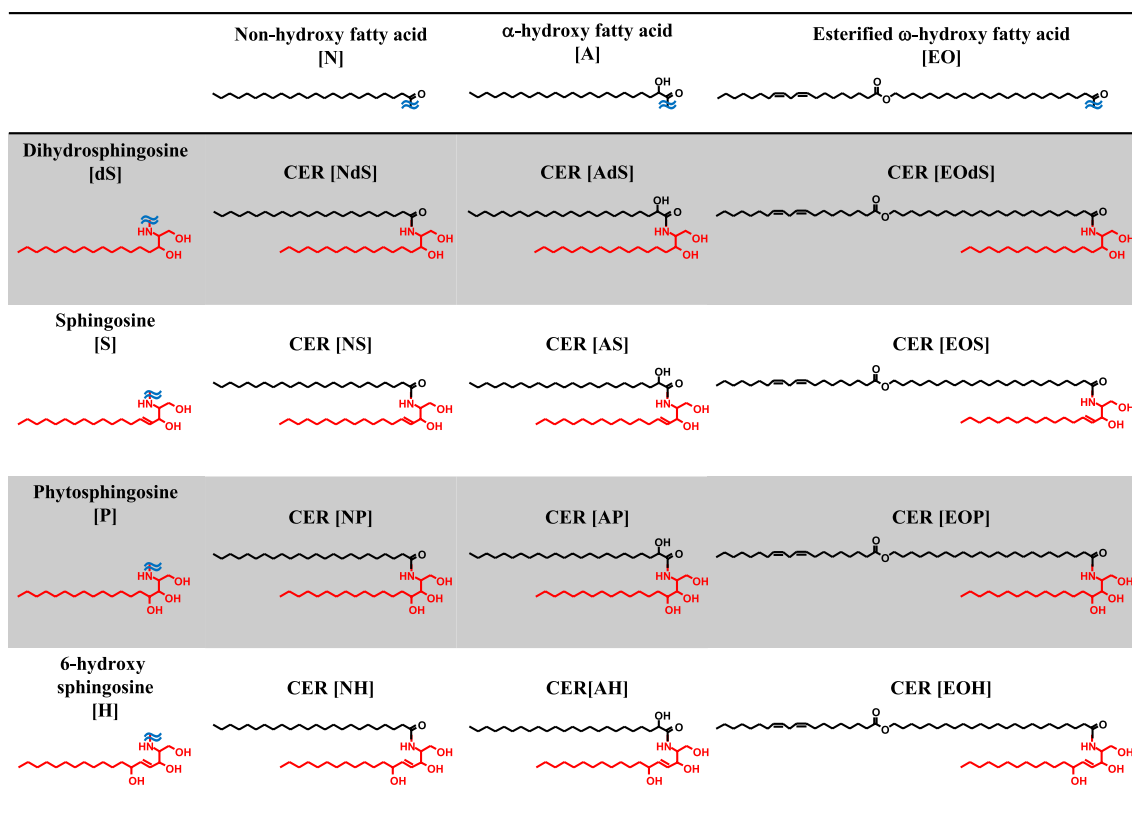

Fig. 1 12 Ceramide subclasses. 12 CERs subclasses existing in all combinations between fatty acids and sphingosine chains are denoted as follows: non-hydroxy fatty acid/dihydrosphingosine base ceramide; [NdS], α-hydroxy fatty acid/dihydrosphingosine base ceramide; CER [AdS], esterified ω-hydroxy fatty acid/dihydrosphingosine base ceramide; CER [EOdS], non-hydroxy fatty acid/sphingosine base ceramide; CER [NS], α-hydroxy fatty acid/sphingosine base ceramide; CER [AS], esterified ω-hydroxy fatty acid/sphingosine base cera- mide; CER [EOS], non-hydroxy fatty acid/phytosphingosine cer- amide; CER [NP], α-hydroxy fatty acid/phytosphingosine base cera- mide; CER [AP], esterified ω-hydroxy fatty acid/ phytosphingosine base ceramide; CER [EOP], non-hydroxy fatty acid/6-hydroxy-sphin- gosine base ceramide; CER [NH], α-hydroxy fatty acid/6-hydroxy- sphingosine base ceramide; [AH], and esterified ω-hydroxy fatty acid/ 6-hydroxy-sphingosine base ceramide; CER [EOH]

CERs [N (18) dS (18)] and [A (16) dS (18)] were provided by Takasago International Corporation (Tokyo, Japan). CERs [N (18) P (18)], [A (18) P (18)], [E (18:2) O (27) S (18)], [E (18:2) O (30) S (18)], [E (18:2) O (27) P (18)], and [E (18:2) O (30) P (18)] were purchased from Evonic Japan (Tokyo, Japan). *N*-omega-CD3-Octadecanoyl-D-erythro-dihydrosphingosine [D-N (18) dS (18)] was purchased from Matreya, LLC (State College, PA, USA). Standard fatty acids, palmitic acid (C16:0-FFA), stearic acid (C18:0-FFA), palmitoleic acid (C16:1-FFA), oleic acid (C18:1-FFA), linoleic acid (C18:2-FFA), arachidic acid (C20:0-FFA) behenic acid (C22:0-FFA), lignoceric acid (C24:0-FFA), cerotic acid (C26:0-FFA), montanic acid (C28:0-FFA), and melissic acid (C30:0-FFA) were purchased from Sigma-Aldrich Japan (Tokyo, Japan). LC/MS-grade methanol and isopropanol for use as the mobile phase in UPLC-TOFMS were purchased from Kanto Chemical Co., Inc. (Tokyo, Japan). All other chemicals used were of reagent-grade quality.

SC lipid extraction from tape-stripped samples

Each of the fifth tape-stripped tapes corresponding to each sampling time point was cut into half using surgical scissors and immersed into a tube containing 5 mL of methanol, placed on a 3D flower Mini-Shaker (Funakoshi Co., Ltd., Tokyo, Japan), and sonicated for 10 min. The solvent was dried under the flowing nitrogen gas. The residual substance was dissolved in 500 μL of methanol/chloroform (95/5 v/v) solution and filtered through a 0.2-μm polytetrafluoroethylene syringe-filter (EKICRODISK13CR, Nihon Pall Ltd., Tokyo, Japan) to remove the insoluble products.

Each filtered sample was injected into the UPLC-TOFMS following the method described below. The remaining half of the fifth stripped tape was used for the protein analysis as described below.

Lipid analysis using UPLC-TOFMS

The intercellular SC lipids on the adhesive tape were analyzed using the protocols reported by t'Kindt, with some modifications [23]. A high-resolution ultraperformance liquid chromatography electrospray spray ionization tandem mass spectrometry (UPLC–ESI–MS/MS) analysis was performed using an ACQUITY UPLC I-class system (Waters, Milford, MA, USA) connected to Xevo G2-XS Q-TOF mass spectrometer (Waters). An ACQUITY UPLC BEH C18 column (1.7 μm, 100 mm × 2.1 mm i.d., Waters, Tokyo) was used at a flow rate of 0.5 mL/min at 80 °C. Elution was performed using a gradient of (A) 20 mM ammonium formate pH 5 and (B) methanol, with a shift from 70% B to 100% B over 75 min (reverse phase methodology). The flow rate was 0.5 mL/min, and the injection volume was 10 μL. The entire system was allowed to re-equilibrate under the starting conditions for 20 min. The instrument was operated in a negative ion electrospray mode. The settings of the ESI source and mass spectrometer were as follows: capillary voltage, 3.00 kV; sampling cone, 20 V; resolving quadrupole LM resolution, 11.0; desolvation gas flow, 1000 L/h; cone gas flow, 50 L/h; collision energy, 22–90 eV using charge state recognition; source temperature, 130 °C; desolvation temperature, 400 °C; detection mode, sensitive; data acquisition, centroid mode from m/z 200 to 1300 at the scan rate of 0.5 s/scan in the full scan.

The ceramide MS/MS data were obtained using a data-independent acquisition program in the mass spectrometer. The collision energy was set at 10–50 V. The mass spectrometer was calibrated using a calibration solution containing sodium formate before the analysis.

To maintain mass accuracy during the analysis, the lock mass of leucine enkephalin (m/z 556.2771 [M+H]+) at the concentration of 0.2 ng/mL was used by a lock spray interface at the flow rate of 5 μL/min.

To visualize the UPLC-TOFMS results in intercellular lipid, a 3D chromatogram of obtained peaks related to intercellular lipid in SC was drawn with MZ mine 2 [24].

Protein analysis in stratum corneum

The amount of SC obtained using the tape methods depended on the patient's specific condition. Therefore, the amounts of stratum corneum lipids (CER, FFA, and CS) were normalized using the total protein amount in this analysis. The amount of protein on the tape was measured by an ortho-phthalaldehyde (OPA) fluorescent protein assay [25].

The remaining half of the fifth stripped tape containing the stripped SC sample was placed into a 1.5-mL Eppendorf tube containing 200 μL of 8 M KOH. The tubes were tightly sealed and heated at 100 °C for 8 h to hydrolyze the proteins in the SC. To prepare the protein standard curve, a 10 mg/mL bovine serum albumin (BSA) standard solution was prepared and diluted to 0, 50, 100, 150, 200, and 250 μg/mL with distilled water and 8 M KOH. The following procedure was conducted under the same conditions. Briefly, 300 μL of 5 M HCl were added to neutralize the samples after cooling them to the room temperature. After centrifugation, the resulting solution was transferred to a 96-well microplate, and 50 μL of OPA reagent was added to each well. Five minutes after the mixing, the fluorescence (excitation, 340 nm; emission, 450 nm) was measured with a 2030 ARVO TMX Multilabel Reader (PerkinElmer Japan, Kanagawa, Japan).

Statistical analysis

Tukey's test was performed to evaluate changes in the intercellular lipid levels after erlotinib administration and the results obtained were used to compare the changes in lipid composition before (day 0) and after erlotinib treatment. A p value < 0.05 was considered as statistically significant. The Pearson correlation coefficient was used to evaluate the associations of the CER [A] and hydroxy fatty acid levels with the dry skin condition after erlotinib administration. Values between 0.7 and 1.0 indicated a strong positive linear relationship via the firm linear rule. The Spearman rank correlation coefficient was used to assess the relationship between the intercellular lipid level and CT-CAE grade after erlotinib administration. An rs value between 0.4 and 0.7 was considered to indicate a positive correlation.

Results

Clinical data summary

Figure 2 presents the changes in the CT-CEA grades of skin rash and dry skin after the erlotinib administration. Notably, the CT-CAE grades of skin rash and dry skin increased with increasing time after the initiation of erlotinib administration.

Intercellular lipid analysis by UPLC-TOFMS after erlotinib administration

UPLC-TOFMS analyses were performed to investigate the effects of erlotinib administration on the intercellular lipid levels in the SC. Normally, lipid extraction employed solvent mixtures containing chloroform, as the solubility of CER in alcohol is not considerably high. Since large amounts of adhesive tape components were eluted with the chloroform containing solvent and these components hinder UPLC-TOFMS analysis, we decided to use methanol as the extraction solvent, which was chloroform-free, based on the study by t'Kindt et al. [23]. The relative extraction percentages of standard materials were 84.2–96.0 %.

A typical total ion current (TIC) chromatogram of intercellular lipids in the SC in ESI mode is shown in Figure S2 (Online Resources 2). The TIC chromatogram exhibited enormous complexity. A previous report indicated that a smooth transition was observed between the lower molecular weight non-esterified CERs (FFAs) and the heavier esterified CERs when using reverse-phase LC methodology [23]. Extracted compound chromatograms (ECC) representing the range of CER features present in CER [NS] (general structure is shown in Fig. 1) with carbon atom numbers of
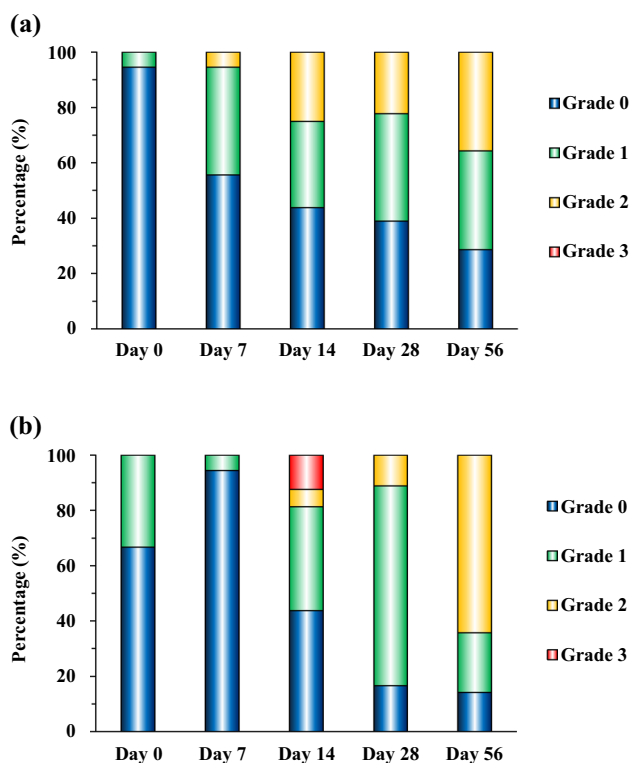

Fig. 2 Changes in **a** skin rash and **b** dry skin grades after the initiation of erlotinib administration according to the CT-CAE ver. 4.0

32–54, and ECCs representing the range of FFA features present in non-hydroxy FFAs with carbon atom numbers of 16–30 are shown in Figure S3 (Online Resources 3). As each individual CER was eluted at a fixed retention time and distance according to differences in the number of CH_2 groups, an increase in the fatty acid chain length induced an elongation of the retention time within the same CER subclass (CER [NS]) and fatty acid groups.

Moreover, different CER subclasses containing the same total carbon numbers were also eluted at a fixed retention time and distance according to differences in the numbers and substituent positions of the OH groups. These differences facilitated the detection of the representatives of all CER subclasses shown. The ECCs representing CER species containing 42 carbon atoms (C42) from different CER subclasses are shown in Figure S4 (Online Resources 4). Although CER [NP], CER [AP] and CER [AS], and CER [NS] and CER [AdS] were (partially) co-eluted, these subclasses could be distinguished by their diagnostic masses. The MS/MS fragmentation pattern enabled the distinction of different isomers, although CER [NH] and CER [AS] are structural isomers. These results are shown in Figures S5 and S6 (Online Resources 5 and 6).

In CER [N(18)H(24)], the m/z values of fragments that did and did not contain a C24 fatty acid chain were

392.38 (green arrow: Fig. S5a) and 253.21 (blue arrow: Fig. S5b), respectively. In contrast, *m/z* values of 408.38 (green arrow: Fig. S6a) and 237.22 (blue arrow: Fig. S6b) were assigned to fragments that did and did not contain the C24 fatty acid chain, respectively, in CER [A(18)S(24)].

Based on the results shown in Figures S2–S6, we assigned a total of 249 CER and 43 FFA molecules in this study. Subsequently, a 3D TOFMS chromatogram of the intercellular lipid compositions from SC extracts was constructed to visualize the results, as shown in Fig. 3. The CERs and FFAs were eluted within 60 min and were assigned. CS was also observed in the chromatogram at approximately 10 min (green arrow in Fig. 3).

The nature of the tape stripping method makes it difficult to control the amount of SC on each adhesive tape strip. Therefore, each peak within the CER and FFA areas on each chromatogram were totaled and normalized to the total protein level in the corresponding tape half in this study. Figures S7 (Online Resources 7) shows the standard curve of protein analysis using an OPA assay. A linear correlation was observed between fluorescence absorbance and protein concentration from 0 to 250 mg/mL ($R^2 = 0.993$).

The changes in the total CER and FFA levels in the SC after the initiation of erlotinib administration are shown in Figure S8 (Online Resources 8). Although both, total CER and FFA levels tended to decrease as the duration of erlotinib administration increased, no statistically significant differences in CER and FFA levels were observed between before and after erlotinib administration.

As skin CERs are classified into 12 subclasses, the changes in CER levels were divided into the 12 subclasses for the analysis; the results are shown in Fig. 4a. No statistically significant changes in the levels of CER [NdS], [NS], [NP], [NH], [AdS], [AS], [EOdS], [EOS], [EOP], and [EOH] were observed. Only the levels of the CER [AP] and [AH] subclasses were changed significantly after the erlotinib administration ($p < 0.05$).

Figure 4b, c depict the changes in different fatty acid subclass levels after the erlotinib administration. The levels in saturated FFAs, which are included in the chemical structure of the CER [N] subclass, and the unsaturated FFA levels were not significantly decreased after the initiation of erlotinib administration. However, the hydroxy FFA levels were lower on day 56 relative to those on days 0 and 7 (Fig 4c). Figure 4d presents the changes in CS levels after erlotinib administration. Notably, the CS levels in the SC increased from baseline overtime after the initiation of erlotinib administration (Fig. 4d). In healthy subjects, these changes in intercellular lipid levels were not observed at 56 days after the initiation of tape stripping (Fig. S9 and S10; Online Resources 9 and 10).

Relationship between CER [A] subclass and hydroxy fatty acid levels

The CER [A] subclass molecular structures include α-hydroxy fatty acids. Therefore, the association between the CER[A] subclass and hydroxy fatty acid levels after erlotinib administration was investigated. Our measurements demonstrated an association between the CER [A] subclass level and the hydroxy FFA level after erlotinib administration (Fig. 5).

Relationship between changes in intercellular lipid component levels in SC and clinical symptoms according to the CT-CAE

To investigate the associations between skin toxicity after erlotinib administration and changes in the levels of intercellular lipid components, the relationship between the CS

Fig. 3 Three-dimensional time-of-flight mass spectrometry chromatogram of the composition of stratum corneum lipid extracts
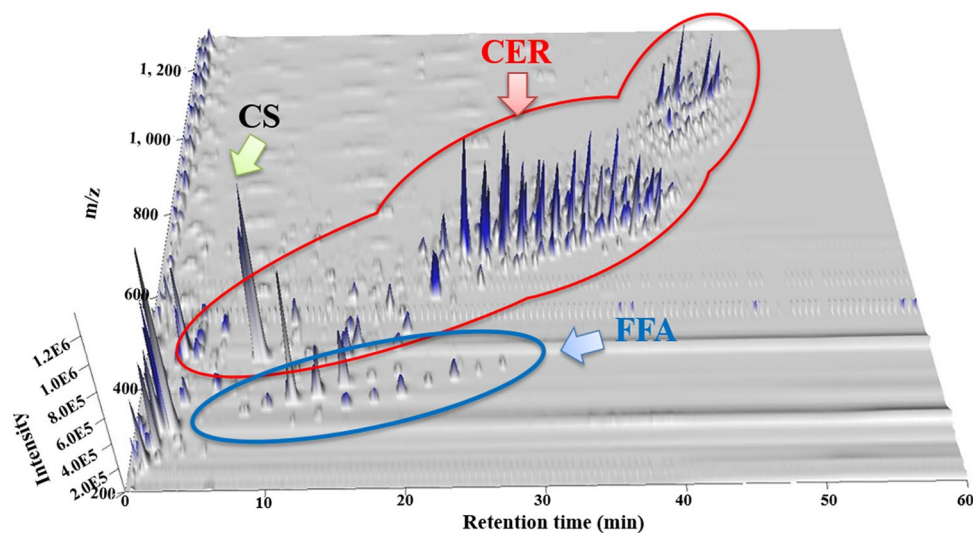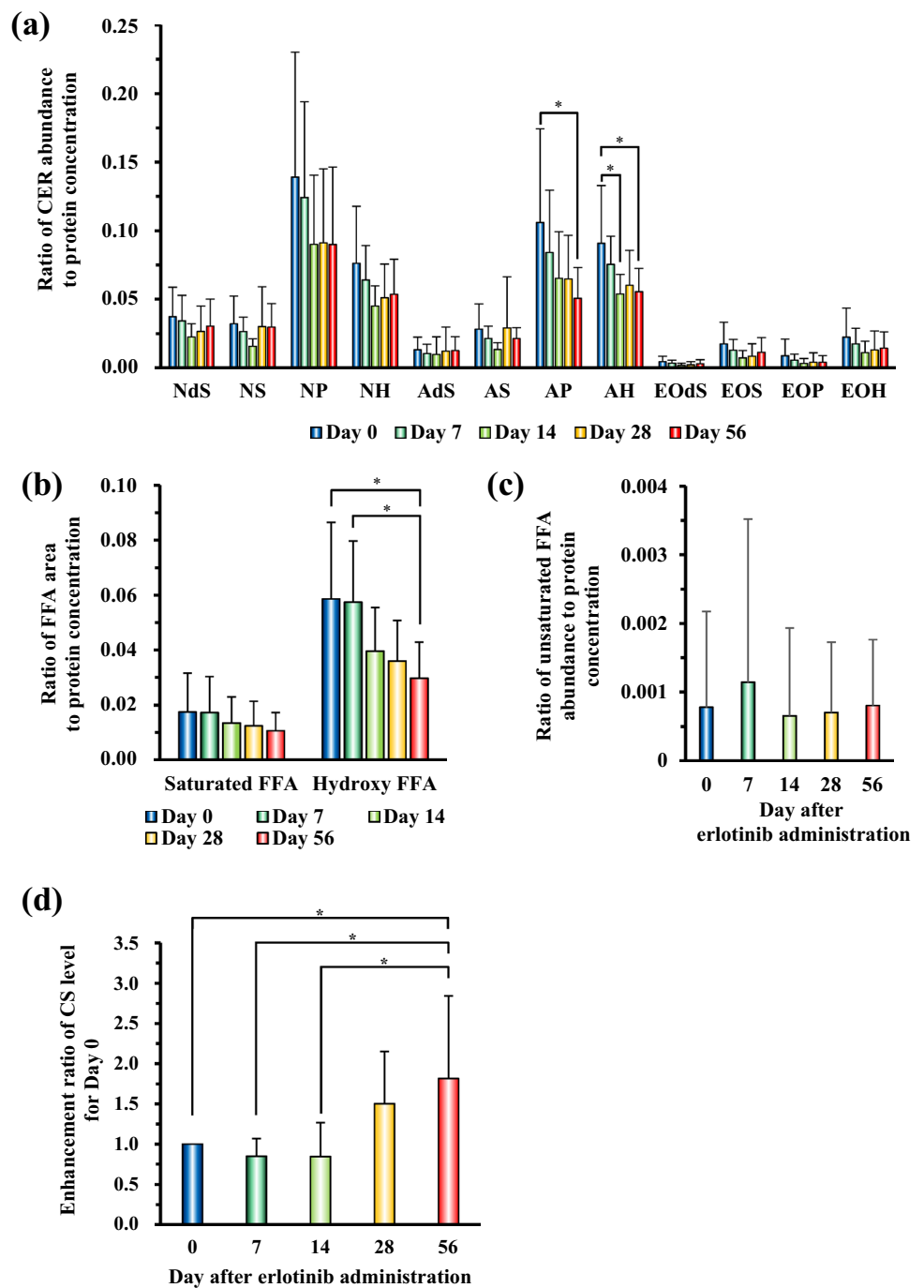
Fig. 4 Changes in **a** ceramide (CER) subclass, **b** free fatty acid (FFA) subclass, **c** unsaturated FFA subclass, and **d** cholesterol sulfate (CS) levels after the initiation of erlotinib administration

level in SC and the clinical symptoms of dry skin and skin rash according to the CT-CAE was evaluated on days 14, 28, and 56 after erlotinib administration. The results are shown in Fig. 6. Although no significant correlation was observed

between clinical symptoms according to the CT-CAE and the CS levels in the SC on day 14 (Fig. 6a), a good correlation was observed between these variables on days 28 and 56 after erlotinib administration (Fig. 6b, c). Regarding the
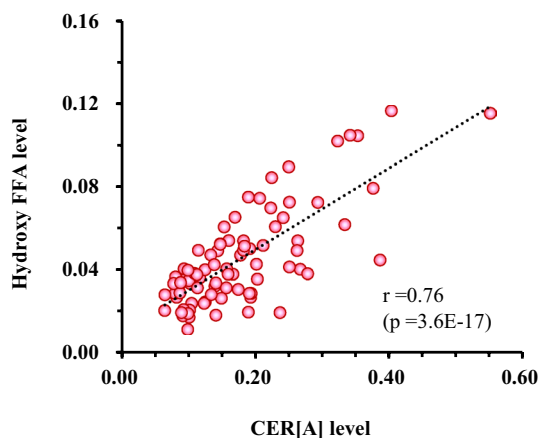
Fig. 5 Association between ceramide (CER) [A] and hydroxy fatty acid levels after the initiation of erlotinib administration

CER [A] subclass and hydroxy FFA levels, no statistically significant correlations were observed between either of these and dry skin symptoms at any time point after erlotinib administration (Fig. S11; Online Resource 11). Similarly, no significant correlation was observed between either the CS, CER [A], or hydroxy FFA levels in the SC with a skin rash (Fig. S12 and Fig. S13; Online Resources 12 and 13).

Discussion

In this study, we investigated whether erlotinib treatment-induced skin toxicity by affecting the intercellular lipid composition in SC. The SC lipid composition in patients who received erlotinib had changed. However, the SC lipid composition had not changed within 56 days in healthy subjects (Fig. S10; Online Resources 10). Their results indicated that erlotinib induces skin toxicity owing to changes in the composition of SC.

CER and FFA are two major intercellular lipid components in SC. CER is a structural backbone of sphingolipids and is composed of a long-chain base and an FFA. An in vitro study reported that epidermal growth factor (EGF) suppressed the expression of critical genes in the sphingolipid and ceramide biosynthetic pathway [26]. In this study, CER[AP], [NP], [AH] and [NH] were decreased in response to the EGF treatment. Furthermore, various fatty acids (mostly C16–C24) can be modified into 2-hydroxylated fatty acids by fatty acid 2-hydroxylase (FA2H) [27]. The FA2H level was also decreased by EGF treatment; kinase inhibitors including erlotinib can induce unanticipated effects caused by the inhibition of off-target kinases [28, 29]. Reports suggested that erlotinib almost completely inhibited the EGFR when used in clinical doses [28]. Therefore, we can assume that erlotinib treatment-induced
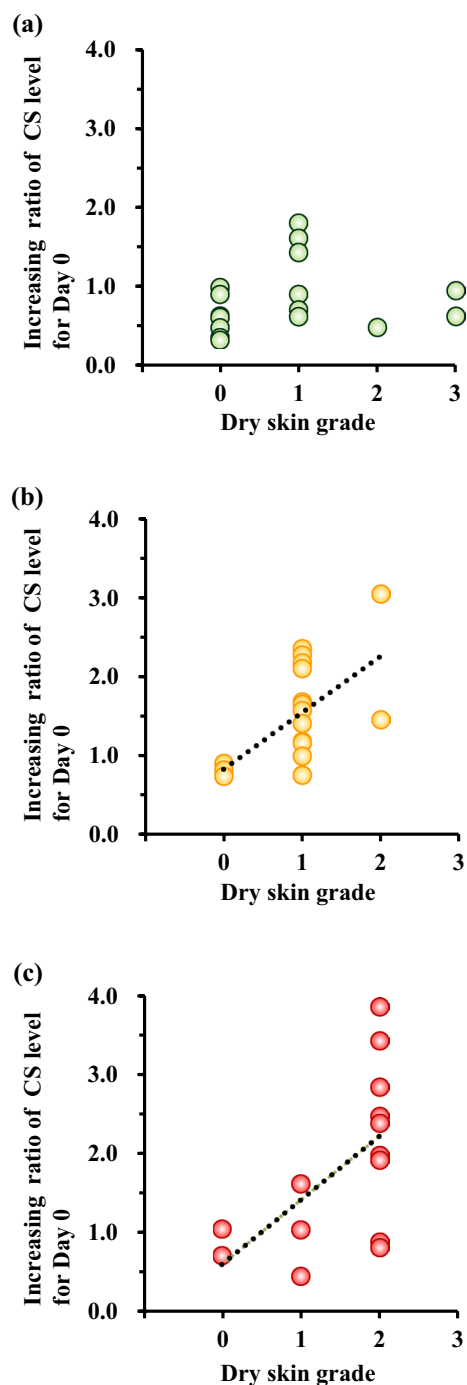

Fig. 6 Relationship between the cholesterol sulfate (CS) level and dry skin grade according to the CT-CAE ver. 4.0 on **a** day 14, **b** day 28, and **c** day 56 after the initiation of erlotinib administration

off-target effects, reducing the activity of the ceramide biosynthetic pathway and activity of FA2H, by altering various signaling pathways and reducing the CER[AP] and [AH].

During the keratinization process, CS is generated by the sulfation of cholesterol via cytosolic sulfotransferases (SULTs) during the transition from the stratum basale to

stratum granulosum [30]. SULT2B1b is a SULT family enzyme, that is expressed in the epidermis and in keratinocytes [31]. CS is then desulfated by steroid sulfatase (SSase) during the transition from the stratum granulosum to the SC. Therefore, it may be speculated that the increased CS level in the SC would be mediated by an increase in SULT2B1b activity or decrease in SSase activity. Previously, a remarkable increase in the CS level in SC was shown to disrupt the skin barrier in patients with X-linked ichthyosis when compared with healthy individuals [32, 33]. However, no significant decrease in SSase activity was observed in patients with X-linked ichthyosis. Lamellar phase separation and an excess of CS in the SC have been observed in patients with X-linked ichthyosis from the results of electron microscopy [34]. In a model lipid membrane study, Rehfeld et al. reported that a high level of CS-induced lamellar phase separation [35]. Furthermore, CS addition to the SC in the healthy volunteers induced the lamellar phase separation [36]. These findings suggest that an excess of CS accelerates phase separation. In our study, the CS level in SC was significantly increased after erlotinib administration and was associated with the dry skin grade according to CT-CAE ver. 4.0. However, no relationship was observed between either the CER or FFA level and dry skin grade, indicating that only the CS level in the SC strongly affected the dry skin condition. These results indicated that the elevated CS levels in the SC in response to erlotinib administration induced phase separation, which in turn caused the dry skin condition.

Retinoic acid, which inhibits differentiation, was also reported to inhibit cholesterol sulfotransferase activity, whereas PPARα, PPARβ/δ, PPARγ, and LXR activators, which stimulate differentiation, enhanced increased SULT-2Blb expression and cholesterol sulfotransferase activity [37–39]. In a molecular dynamic simulation study, Mazumder reported that erlotinib may act as a ligand for PPARγ [40]. Therefore, we assumed that PPARγ was activated by erlotinib and PPARγ-mediated signaling enhanced the expression of SULT2Blb, which in turn induced the increase in CS in the SC.

Reports suggested that dry skin conditions (conductance, dryness, roughness, and scaliness) strongly correlated with the level of CER [NP], and CER [NH] [41]. Vyumvuhore et al. reported that the CER [NS], [NdS], and [EOP] subclasses were decreased in the SC in healthy volunteers with dry skin relative to those without dry skin condition [14]. Schreiner et al. also reported decreased levels in the CER [EOS] and [EOH] ratios and increased level in CER [NS] and [AS] in dry skin SC [42]. From the in vitro results, EGF treatment also led to the decreased levels of CER [NP], CER [NP] and CER [EOS] [26]. Although CER [NP] and CER [NH] had a tendency to get significantly decreased after erlotinib administration in our study, no significant differences

were observed. These results indicated that the individual difference was large and no significant difference was observed. In this study, decrease in the levels of other CER subclasses ([AP] and [AH]) were observed after erlotinib administration. Moreover, the CS level in SC was clearly increased. Their results strongly indicate that the SC condition in erlotinib treatment-associated dry skin differed from that in other types of dry skin.

The grade of dry skin symptoms had also been increased after erlotinib administration in our study, which is in agreement with the previous clinical study [43]. In our study, all SC samples were collected from the inner arm. Although skin condition in the inner arm was not a lesion part in some of the patients, the composition of intercellular lipids in the SC was clearly altered. Moreover, the change of SC lipid composition at the inner arm tended to start from day 14, as was evident from the results in Fig. 4. Since orally administered erlotinib is distributed in the systemic body through the blood flow, our current study suggested that the change in the lipid composition at the inner arm reflected the systemic dry skin symptoms. Therefore, it was strongly suggested that SC lipid analysis with tape stripping from inner forearm was one of the superior methods to evaluate the dry skin symptom.

Currently, emollients and topical steroids are the main treatment options for EGFR-TKI-induced skin toxicity, including dry skin condition. Our results suggest that application of topical medications, including components that may improve the intercellular lipid levels, may be useful.

The in vitro results obtained by Tran et al. agree with the in vivo clinical symptoms shown in our study [26]. Since they investigated the effect of EGF treatment on the CER biosynthetic pathway, we speculate that the results of our current study in erlotinib can be applied to the treatment of skin toxicity induced by other EGFR-TKIs.

In conclusion, this study investigated changes in the intercellular lipid components (CER, FFA, and CS) in response to erlotinib administration. Notably, the levels of the CER subclasses [AP] and [AH] and hydroxy FFAs were decreased after the initiation of erlotinib administration, whereas the level of CS was increased. As the increase in the CS level was associated with the dry skin grade according to the CT-CAE, we conclude that a higher CS level in the SC caused erlotinib-related dry skin.

Author contributions TU, KA, HY designed and directed the project. YM, TS, YS, MM, MK and YK developed the trial design. HF, DK and TS performed the experiments and they analyzed data. HM and KT verified the analytical methods of intercellular lipid extract from SC with UPLC-TOFMS. TU and HF and DK drafted the manuscript

and designed the figures. All authors contributed to the writing of the final manuscript.

Availability of data and material The datasets generated and/or analyzed during the current study are available from the corresponding author on reasonable request.

Code availability Not applicable.

Compliance with ethical standards

Conflict of interest The authors declare no conflicts of interest associated with this manuscript.

Ethics approval The study protocols were approved by the Institutional Review Boards of Shizuoka General Hospital (approval number: SGH 14-09-35) and the University of Shizuoka (approval number: 28-41, 29-47). This study was registered at UMIN-CTR under the study ID UMIN 000020675.

References

1. Yewale C, Baradia D, Vhora I, Patil S, Misra A (2013) Epidermal growth factor receptor targeting in cancer: a review of trends and strategies. Biomaterials 34(34):8690–8707. https://doi.org/10.1016/j.biomaterials.2013.07.100
2. Guggina LM, Choi AW, Choi JN (2017) EGFR inhibitors and cutaneous complications: a practical approach to management. Oncol Ther 5(2):135–148. https://doi.org/10.1007/s40487-017-0050-6
3. Kiyohara Y, Yamazaki N, Kishi A (2013) Erlotinib-related skin toxicities: treatment strategies in patients with metastatic non-small cell lung cancer. J Am Acad Dermatol 69(3):463–472. https://doi.org/10.1016/j.jaad.2013.02.025
4. Kozuki T (2016) Skin problems and EGFR-tyrosine kinase inhibitor. Jpn J Clin Oncol 46(4):291–298. https://doi.org/10.1093/jjco/hyv207
5. Potthoff K, Hofheinz R, Hassel JC, Volkenandt M, Lordick F, Hartmann JT, Karthaus M, Riess H, Lipp HP, Hauschild A, Trarbach T, Wollenberg A (2011) Interdisciplinary management of EGFR-inhibitor-induced skin reactions: a German expert opinion. Ann Oncol 22(3):524–535. https://doi.org/10.1093/annonc/mdq387
6. Baroni A, Buommino E, De Gregorio V, Ruocco E, Ruocco V, Wolf R (2012) Structure and function of the epidermis related to barrier properties. Clin Dermatol 30(3):257–262. https://doi.org/10.1016/j.clindermatol.2011.08.007
7. Feingold KR, Elias PM (2014) Role of lipids in the formation and maintenance of the cutaneous permeability barrier. Biochim Biophys Acta BBA Mol Cell Biol Lipids 3:280–294. https://doi.org/10.1016/j.bbalip.2013.11.007
8. Proksch E, Fölster-Holst R, Jensen J-M (2006) Skin barrier function, epidermal proliferation and differentiation in eczema. J Dermatol Sci 43(3):159–169. https://doi.org/10.1016/j.jdermsci.2006.06.003
9. Pilgram GSK, Vissers DCJ, Van Der Meulen H, Koerten HK, Pavel S, Lavrijsen SPM, Bouwstra JA (2001) Aberrant lipid organization in stratum corneum of patients with atopic dermatitis and lamellar ichthyosis. J Investig Dermatol 117(3):710–717. https://doi.org/10.1046/j.0022-202x.2001.01455.x
10. Coderch L, Lopez O, de la Maza A, Parra JL (2003) Ceramides and skin function. Am J Clin Dermatol 4(2):107–129. https://doi.org/10.2165/00128071-200304020-00004
11. Van Smeden J, Boiten WA, Hankemeier T, Rissmann R, Bouwstra JA, Vreeken RJ (2014) Combined LC/MS-platform for analysis of all major stratum corneum lipids, and the profiling of skin substitutes. Biochim Biophys Acta BBA Mol Cell Biol Lipids 1841(1):70–79. https://doi.org/10.1016/j.bbalip.2013.10.002
12. Harding CR (2004) The stratum corneum: structure and function in health and disease. Dermatol Ther 17(s1):6–15. https://doi.org/10.1111/j.1396-0296.2004.04s1001.x
13. Engelke M, Jensen JM, Ekanayake-Mudiyanselage S, Proksch E (1997) Effects of xerosis and ageing on epidermal proliferation and differentiation. Br J Dermatol 137(2):219–225. https://doi.org/10.1046/j.1365-2133.1997.18091892.x
14. Vyumvuhore R, Michael-Jubeli R, Verzeaux L, Boudier D, Le Guillou M, Bordes S, Libong D, Tfayli A, Manfait M, Closs B (2018) Lipid organization in xerosis: the key of the problem? Int J Cosmet Sci 40(6):549–554. https://doi.org/10.1111/ics.12496
15. Meckfessel MH, Brandt S (2014) The structure, function, and importance of ceramides in skin and their use as therapeutic agents in skin-care products. J Am Acad Dermatol 71(1):177–184. https://doi.org/10.1016/j.jaad.2014.01.891
16. van Smeden J, Janssens M, Kaye EC, Caspers PJ, Lavrijsen AP, Vreeken RJ, Bouwstra JA (2014) The importance of free fatty acid chain length for the skin barrier function in atopic eczema patients. Exp Dermatol 23(1):45–52. https://doi.org/10.1111/exd.12293
17. Albanell J, Rojo F, Averbuch S, Feyereislova A, Mascaro JM, Herbst R, LoRusso P, Rischin D, Sauleda S, Gee J, Nicholson RI, Baselga J (2002) Pharmacodynamic studies of the epidermal growth factor receptor inhibitor ZD1839 in skin from cancer patients: histopathologic and molecular consequences of receptor inhibition. J Clin Oncol 20(1):110–124. https://doi.org/10.1200/jco.2002.20.1.110
18. Lacouture ME (2006) Mechanisms of cutaneous toxicities to EGFR inhibitors. Nat Rev Cancer 6(10):803–812. https://doi.org/10.1038/nrc1970
19. Nanba D, Toki F, Barrandon Y, Higashiyama S (2013) Recent advances in the epidermal growth factor receptor/ligand system biology on skin homeostasis and keratinocyte stem cell regulation. J Dermatol Sci 72(2):81–86. https://doi.org/10.1016/j.jdermsci.2013.05.009
20. Clausen M-L, Slotved HC, Krogfelt KA, Agner T (2016) Tape stripping technique for stratum corneum protein analysis. Sci Rep 6:19918–19918. https://doi.org/10.1038/srep19918
21. Motta S, Monti M, Sesana S, Caputo R, Carelli S, Ghidoni R (1993) Ceramide composition of the psoriatic scale. Biochim Biophys Acta BBA Mol Basis Dis 1182(2):147–151. https://doi.org/10.1016/0925-4439(93)90135-n
22. Masukawa Y, Narita H, Shimizu E, Kondo N, Sugai Y, Oba T, Homma R, Ishikawa J, Takagi Y, Kitahara T, Takema Y, Kita K (2008) Characterization of overall ceramide species in human-stratum corneum. J Lipid Res 49(7):1466–1476. https://doi.org/10.1194/jlr.m800014-jlr200
23. t'Kindt R, Jorge L, Dumont E, Couturon P, David F, Sandra P, Sandra K (2012) Profiling and characterizing skin ceramides using reversed-phase liquid chromatography-quadrupole time-of-flight mass spectrometry. Anal Chem 84(1):403–411. https://doi.org/10.1021/ac202646v
24. Pluskal T, Castillo S, Villar-Briones A, Orešič M (2010) MZmine 2: modular framework for processing, visualizing, and analyzing mass spectrometry-based molecular profile data. BMC Bioinform 11(1):395. https://doi.org/10.1186/1471-2105-11-395

25. Go K, Horikawa Y, Garcia R, Villarreal FJ (2008) Fluorescent method for detection of cleaved collagens using O-phthaldialdehyde (OPA). J Biochem Biophys Methods 70(6):878–882. https://doi.org/10.1016/j.jbbm.2007.05.004

26. Tran QT, Kennedy LH, Leon Carrion S, Bodreddigari S, Goodwin SB, Sutter CH, Sutter TR (2012) EGFR regulation of epidermal barrier function. Physiol Genom 44(8):455–469. https://doi.org/10.1152/physiolgenomics.00176.2011

27. Hama H (2010) Fatty acid 2-Hydroxylation in mammalian sphingolipid biology. Biochim Biophys Acta BBA Mol Cell Biol Lipids 1801(4):405–414. https://doi.org/10.1016/j.bbalip.2009.12.004

28. Yamamoto N, Honma M, Suzuki H (2011) Off-target serine/threonine kinase 10 inhibition by erlotinib enhances lymphocytic activity leading to severe skin disorders. Mol Pharmacol 80(3):466–475. https://doi.org/10.1124/mol.110.070862

29. Vandyke K, Fitter S, Dewar AL, Hughes TP, Zannettino AC (2010) Dysregulation of bone remodeling by imatinib mesylate. Blood 115(4):766–774. https://doi.org/10.1182/blood-2009-08-237404

30. Elias PM, Williams ML, Choi EH, Feingold KR (2014) Role of cholesterol sulfate in epidermal structure and function: lessons from X-linked ichthyosis. Biochem Biophys Acta 1841(3):353–361. https://doi.org/10.1016/j.bbalip.2013.11.009

31. Higashi Y, Fuda H, Yanai H, Lee Y, Fukushige T, Kanzaki T, Strott CA (2004) Expression of cholesterol sulfotransferase (SULT2B1b) in human skin and primary cultures of human epidermal keratinocytes. J Investig Dermatol 122(5):1207–1213. https://doi.org/10.1111/j.0022-202X.2004.22416.x

32. Elias PM, Williams ML, Maloney ME, Bonifas JA, Brown BE, Grayson S, Epstein EH Jr (1984) Stratum corneum lipids in disorders of cornification. Steroid sulfatase and cholesterol sulfate in normal desquamation and the pathogenesis of recessive X-linked ichthyosis. J Clin Investig 74(4):1414–1421. https://doi.org/10.1172/jci111552

33. Williams ML, Elias PM (1981) Stratum corneum lipids in disorders of cornification: increased cholesterol sulfate content of stratum corneum in recessive x-linked ichthyosis. J Clin Investig 68(6):1404–1410. https://doi.org/10.1172/jci110391

34. Elias PM, Crumrine D, Rassner U, Hachem JP, Menon GK, Man W, Choy MH, Leypoldt L, Feingold KR, Williams ML (2004) Basis for abnormal desquamation and permeability barrier dysfunction in RXLI. J Investig Dermatol 122(2):314–319. https://doi.org/10.1046/j.1523-1747.2003.22258.x

35. Rehfeld SJ, Williams ML, Elias PM (1986) Interactions of cholesterol and cholesterol sulfate with free fatty acids: possible relevance for the pathogenesis of recessive X-linked ichthyosis. Arch Dermatol Res 278(4):259–263. https://doi.org/10.1007/bf00407734

36. Zettersten E, Man M-Q, Farrell A, Ghadially R, Williams ML, Feingold KR, Elias PM, Sato J, Denda M (1998) Recessive x-linked ichthyosis: role of cholesterol-sulfate accumulation in the barrier abnormality. J Investig Dermatol 111(5):784–790. https://doi.org/10.1046/j.1523-1747.1998.00386.x

37. Jetten AM, George MA, Pettit GR, Herald CL, Rearick JI (1989) Action of phorbol esters, bryostatins, and retinoic acid on cholesterol sulfate synthesis: relation to the multistep process of differentiation in human epidermal keratinocytes. J Investig Dermatol 93(1):108–115. https://doi.org/10.1111/1523-1747.ep12277374

38. Jiang YJ, Kim P, Elias PM, Feingold KR (2005) LXR and PPAR activators stimulate cholesterol sulfotransferase type 2 isoform 1b in human keratinocytes. J Lipid Res 46(12):2657–2666. https://doi.org/10.1194/jlr.M500235-JLR200

39. Jetten AM, George MA, Nervi C, Boone LR, Rearick JI (1989) Increased cholesterol sulfate and cholesterol sulfotransferase activity in relation to the multi-step process of differentiation in human epidermal keratinocytes. J Investig Dermatol 92(2):203–209. https://doi.org/10.1111/1523-1747.ep12276731

40. Mazumder M, Ponnan P, Das U, Gourinath S, Khan HA, Yang J, Sakharkar MK (2017) Investigations on binding pattern of kinase inhibitors with PPARgamma: molecular docking, molecular dynamic simulations, and free energy calculation studies. PPAR Res 2017:6397836. https://doi.org/10.1155/2017/6397836

41. Ishikawa J, Yoshida H, Ito S, Naoe A, Fujimura T, Kitahara T, Takema Y, Zerweck C, Grove GL (2013) Dry skin in the winter is related to the ceramide profile in the stratum corneum and can be improved by treatment with a Eucalyptus extract. J Cosmet Dermatol 12(1):3–11. https://doi.org/10.1111/jocd.12019

42. Schreiner V, Pfeiffer S, Lanzendörfer G, Wenck H, Diembeck W, Gooris GS, Proksch E, Bouwstra J (2000) Barrier characteristics of different human skin types investigated with X-ray diffraction, lipid analysis, and electron microscopy imaging. J Investig Dermatol 114(4):654–660. https://doi.org/10.1046/j.1523-1747.2000.00941.x

43. Goto K, Nishio M, Yamamoto N, Chikamori K, Hida T, Maemondo M, Katakami N, Kozuki T, Yoshioka H, Seto T, Fukuyama T, Tamura T (2013) A prospective, phase II, open-label study (JO22903) of first-line erlotinib in Japanese patients with epidermal growth factor receptor (EGFR) mutation-positive advanced non-small-cell lung cancer (NSCLC). Lung Cancer 82(1):109–114. https://doi.org/10.1016/j.lungcan.2013.07.003

Publisher's Note Springer Nature remains neutral with regard to jurisdictional claims in published maps and institutional affiliations.